Design of Hierarchal 3D Metal Oxide Structures for Water Oxidation and Purification

Mahmud Diab, Karam Shreteh, Noa Afik, Michael Volokh, Sigal Abramovich, Uri Abdu and Taleb Mokari*

Dr. Mahmud Diab, Karam Shreteh, Noa Afik, Dr. Michael Volokh, and Prof. Taleb Mokari
Department of Chemistry, Ben-Gurion University of the Negev, 8410501, Israel
E-mail: mokari@bgu.ac.il

Prof. Sigal Abramovich
Department of Geological & Environmental Sciences, Ben-Gurion University of the Negev, 8410501, Israel

Prof. Uri Abdu
Department of Life Sciences, Ben-Gurion University of the Negev, 8410501, Israel

Abstract
Given their unique properties, tremendous progress has been realized in the use of nanostructured materials for various applications. However, their incorporation and fabrication into prototypic devices remain challenging due to their limited ability to form hierarchical three-dimensional (3D) structures through the use of large scale, low cost, and facile processes. Herein, we address this challenge and demonstrate the growth of unique hierarchical structures by coating calcareous foraminiferal shells with metal oxide materials *via* simple and inexpensive processes conducted on a large scale. Foraminifera are highly diverse and abundant marine unicellular protists surrounded by large, ranging from 0.1 mm to more than 200 mm in size, identical porous and complex hierarchical shells. In the present study, these hierarchal structures were investigated in electrochemical water oxidation reactions and tested in terms of their ability to purify water from inorganic (metal ions) contaminates. The remarkable performances of the prototype filters and catalysts developed here, among the best recorded values in both fields, are reported. These findings thus open new perspectives for catalytic and water purification applications.

Body of communication

Hierarchical 3-dimensional (3D) nanostructures are widely recognized and during the past two decades, this field has witnessed a rapid rise in interest due to the unique properties of such structures. Still, a persistent need for such materials remains. Indeed, the limited success realized in forming hierarchical structures of inorganic materials (HSIMs) is one of the major obstacles preventing technological progress in various applications involving such moieties, such as catalysis, capacitors, battery, purification technology, and electronics. Major efforts for fabricating well-defined 3D structures have primarily focused on four different routes, namely photo/electro lithography, assembly, 3D printing, and template-mediated methods, with various structures having been obtained through those techniques at high quality/yield.[1] However, these methods suffer from high costs, difficulty in fabricating free-standing structures and, in some cases, limited throughput.[2,3] On the other hand, templated approaches are usually facile, relatively inexpensive, and are able to produce complex structures. In considering templates, several fascinating microorganisms display highly ordered and complex structures, such as viruses, bacteria, fungi, diatoms, and foraminifera that cannot be easily mimicked artificially.[4,5] Relative to synthetic materials, hardened biological materials offer clear advantages, given the ability of living organisms to engineer and fabricate materials with structures and dimensions that are very challenging to achieve in traditional methods, thereby offering a wide spectrum of applied possibilities. Furthermore, such organisms accurately replicate their structures and functionalities during evolution, which is crucial for their survival. These properties overcome issues related to the reproducibility of these identical and unique structures and can facilitate their use in high quality commercial products. Nevertheless, a clear disadvantage of using natural materials, especially those comprising a single component is that they usually suffer from poor inherent properties and, therefore, post-treatment processes are required to attain multi-functionalities. Thus, the combination of the natural template and introduced synthetic capabilities can be used to rationally create 3D structures with increased functionalities.

To date, extensive research on the use of microorganism shells as templates for forming various 3D morphologies for different applications has been reported.[3,6,7,8] Several approaches describing the deposition/growth of nanomaterials on such templates, such as gas phase hydrothermal reactions, photoreduction, sonochemical processes, sputtering, and others have been described.[9,10,11] The Mann group was able to form inorganic nanotubes (FeO, CdS, and PbS) with deposition of metallic nanoparticles (such as Pt, Ag, and Au) using the tobacco mosaic virus (TMV) as template.[11,12] Kern and co-workers expanded the use of TMV for the

formation of Ni and Co nanowires.[13] Saraf and colleagues fabricated electrical conducting Au bridges of using the bacteria *Bacillus cereus* as template.[14] Mirkin and co-workers produced a hierarchical structure of Au nanoparticles using fungal templates.[15] In recent decades, substantial efforts have been invested in fabricating a well-defined 3D structures using diatom templates.[16,17,18,19,20,21] For example, Haigh and associates formed a MoS_2 layer using the diatom *Coscinodiscus* as template.[22] Lang et al. expanded the potential application of diatoms by modifying their surface with TiO_2 nanoparticles, and examined the photocatalytic performance.[23]

One interesting group of microorganisms that present a variety of highly porous 3D shell structures is the foraminifera which are vastly diverse and abundant unicellular marine protists, found in all parts of the oceans, from the poles to the equator and from shallow intertidal regions to the deep sea. They formed amongst the most ancient and abundant fossils and their shells (the majority of which is made of calcium carbonate) accumulate in mass quantities in oceanic sediments, thus becoming one of the most important components of sedimentary (carbonate) rocks.[24,25,26] Annual global production of calcium carbonate by foraminifera was estimated as 43 million tons, an amount representing close to 50% of the total annual $CaCO_3$ precipitation in the ocean.

Despite their protist origin, foraminifera are relatively large in size (from 0.1 to more than 200 mm) and are highly complex organisms. One of the most unique characteristics of foraminifera is their ability to build highly mesoporous 3D shells of $CaCO_3$ of various shapes and sizes presenting complex internal and external structures. Surprisingly, despite their unique structures, these structures have not yet been used as templates for growing inorganic materials. In the present study, we harnessed the naturally designed morphologies of calcareous foraminiferal shells (CFS) to rationally form hierarchical structures of nanofeatures. We demonstrate the inexpensive and abundant formation of unique inorganic 3D porous structures using CFS of the benthonic genus *Sorites* as scaffolds. We subsequently examined their performance as an electrocatalyst for water oxidation and as a filter of inorganic containments.

A general and simple approach was developed for the growth of unique hierarchical 3D porous structures which offer metal and metal oxide nanofeatures using CFSs, as portrayed in **Figure 1**. The procedure for growing nanostructures on *Sorites* involved partial removal of the outer $CaCO_3$ shell by transferring the organisms to a solution of 0.05 M HCl for 2–3 min and then washing with water (Figure S1). The removal of the outer layers of the shell allows for the grown materials to reach its interior walls and tunnels. Then, the *Sorites* were placed in different growth solutions for coating with inorganic materials as described in the Experimental

section. Figure 1 presents optical and SEM images of *Sorites* coated with Co (A, E), MnO (B, F), α-Fe$_2$O$_3$ (C, G), and NiO (D, H). The conformal coating of the *Sorites* with different materials enabled for controlling the thickness of the coated materials from a few nanometers to a few micrometers as presented in the high magnification SEM images shown in the insets of Figure 1E, F, G, and H.

The homogeneity of the coating in all samples was confirmed by EDX mapping and XRD characterization, as presented in Figure 1I, J, K and L. All of the coated materials were crystalline and clear peaks of rhombohedral Mg$_{0.1}$Ca$_{0.9}$CO$_3$ and the coating materials (Co, α-Fe$_2$O$_3$, MnO, and NiO) matched the fcc bulk structure. Formation of a new phase of rhombohedral CaCO$_3$ was observed as a result of the heating process. The EDX data collected from all samples revealed that conformal coating had been achieved, as presented in the inset of the XRD patterns in Figure 1.

One of the most appealing advantages of using CFSs as scaffolds to grow various materials is the simplicity of sacrificially removing the scaffold while retaining the morphology. We tested the process of removing the *Sorites* template after its coating by a thick layer of a Co shell. The removal of the template was carried out by first annealing the samples and converting the Co into Co$_3$O$_4$ to provide additional stability and then immersing the *Sorites*@Co$_3$O$_4$ sample in HCl solution (0.1 M) for 20 minutes, followed by washing with distilled water. **Figure 2** shows the process of etching the calcite template coated with Co$_3$O$_4$ material before (Figure 1A) and after (Figure 2A) calcite removal. Removal of the template was confirmed by XRD, which shows that the calcite peaks disappeared after etching and that only Co$_3$O$_4$ peaks could be detected, as shown in Figure 2B (bottom pattern). Figures 2C and 2D present SEM images of a cross-section of samples before and after the etching process, respectively, confirming how the hierarchical structure of the sample was preserved after removing the template. The removal of calcite from the sample was verified by EDX mapping. Before etching, the Ca (red) and Co (blue) signals are clearly shown in Figure 2E, however, after etching, the Ca signal disappeared and only the Co signal was detected, as presented in Figure 2F. This etching process can be easily expanded to other inorganic materials that are stable in mild acidic solution.

One of the great motivations for designing materials in a hierarchical 3D structure configuration is the desire to achieve high surface area. Calculating the surface area of native *Sorites* (after removing the top layer) using the Brunauer-Emmett-Teller (BET) theory yields a value of ~5 m²/g. This value is comparable to the surface area reported for other biological

scaffolds in use (1.4–51 m²/g).[28,29,30,31,32,33,34] Coating *Sorites* with Co followed by etching of the template doubled the surface area of the structures (~8 m²/g).

This high surface area, combined with a hierarchical 3D arrangement, pave the way for the use of *Sorites* in several applications. Here, we focused on the potential of the HSIMs formed in two applications, namely water purification (i.e., removing metal cations) and catalysis (i.e., water oxidation). For both applications, a general requirement is a material with large surface area, an essential factor for creating highly efficient devices. HSIMs possess well-defined traits that make them ideal candidates as catalysts and filters, with the most significant being their high surface area, the accessibility of the reactants/monomers to reach the interior surface of the 3D structures, and that they provide a confined space (nano-reactor) for catalysis that can consequently lead to higher chemical yield/conversion. Finally, various inorganic materials can be grown that offer diverse functionalities.

To study the activity of the HSIMs in removing contaminates from water and in water oxidation catalysis, *Sorites* were coated with abundant inexpensive and non-toxic inorganic materials. In addressing the electrocatalytic properties of the HSIMs, *Sorites*@Co and *Sorites*@NiO were considered as electrocatalysts. **Figure 3** presents a photograph of the electrodes (Figure 3A) and the electrochemical performance (Figure 3B) of the hierarchal structure coated with Co or NiO. The electrodes prepared from *Sorites*@Co (red) or *Sorites*@NiO (blue) showed maximal currents of 154 mA/cm^2 (62 mA/cm^2) and 74 mA/cm^2 (35 mA/cm^2) at 1 V (0.8 V) *vs*. Ag/AgCl and an onset potential of ~0.55 V *vs*. Ag/AgCl, respectively. A control experiment involving an electrode coated with silver paint generated a maximal current of ~2 mA/cm^2 at 1 V *vs*. Ag/AgCl (Figure 3B, black). The reported current density is among the highest electrocatalytic currents obtained using cobalt- and nickel-based materials and the onset potential is comparable with the reported values using the same materials.[35,36,37,38,39,40,41,42] Besides performance, the clear advantage of our electrocatalysts, as compared to the state-of-the-art electrocatalysts, is the simplicity in fabricating the anode, the low quantity of active materials (Co, NiO, or others) needed to achieve high activities due to the formation of 3D structures and the direct costs of the process, which are considerably lower than needed to assemble most cobalt- and nickel-based electrocatalysts.

As the demand for clean water is steeply increasing, developing new structures that can remove metal ions have become more pronounced. With this in mind, we tested whether the HSIMs developed here can be used for removing metal cations (i.e., heavy and non-heavy metal ions) from contaminated water. We first examined the ability of untreated *Sorites* and *Sorites* that had been coated with inorganic layers to remove metal cations from water, as

portrayed in **Figure 4**.[43,44] Figure 4A shows an image of the filter and a schematic illustration of the filtration process. The performance of the filter was examined by passing three different contaminated solutions of dissolved $Pb(ac)_2 \cdot 3H_2O$, $CdCl_2$, or $CuCl_2$, in water through 2 g of active material corresponding to untreated *Sorites* or *Sorites*@inorganic materials in a cylindrical tube. The filtration process was carried out without external pressure. This is a clear advantage, as compared to many commercial filters.

The concentration of metal cations, before and after filtration, was measured by atomic absorption spectroscopy (AAS). Surprisingly, untreated *Sorites* structures, with no surface modification, exhibited remarkable performance. Figure 4C shows that the concentrations of the three cation solutions, before and after the filtration, were reduced significantly. Ten mL of metal solutions containing 136 ppm of Pb^{2+} (Figure 4C, black), 103 ppm of Cd^{2+} (Figure 4C, orange) or 108 ppm of Cu^{2+} (Figure 4C, pink), were passed through the untreated *Sorites*. The concentrations of the metal cations, after filtration, were reduced to <0.02 ppm, 2.7 ppm, and 6.3 ppm of Pb^{2+}, Cd^{2+}, and Cu^{+2}, respectively.

To improve filter performance, we coated the *Sorites* with iron hydroxide (Figure 4B). Iron-based oxides are promising candidate materials for extraction of metal ions from water/wastewater.[45,46,47,48] Iron hydroxide is a particularly interesting material for removing ions due to the high affinity of its hydroxide groups for metal cations ($\equiv FeOH + M^{2+} \rightleftharpoons \equiv FeOM^+ + H^+$).[49] Moreover, iron hydroxide is non-toxic, abundant, inexpensive, and easy to grow (see Experimental section).

When *Sorites*@Fe(OH)$_x$ were used instead of untreated *Sorites*, the purification efficiency was noticeably improved, specifically for Cd^{2+} and Cu^{2+} (using the same initial concentrations of cations that were used in the experiments with untreated *Sorites*). Similar to untreated *Sorites*, the use of *Sorites*@Fe(OH)$_x$ led to a significant decrease in lead concentration following filtration, with levels dropping from 136 ppm to <0.02 ppm (below the detection limit of the instrument), corresponding to the removal of 99.98% of the lead contaminate (Figure 4C, black). Regarding Cd^{2+}, the AAS measurements showed a reduction from 103 ppm to 0.08 ppm after filtration, corresponding to a purification of >99.9% of the cation (Figure 4C, orange). A significant improvement was also recorded for Cu^{2+}, with the concentration being reduced 99.99% from 108 ppm to <0.005 ppm, as shown in Figure 4C (pink).

In summary, we have shown that the design of hierarchical 3D metal oxide structures can be achieved using calcareous foraminiferal shells as scaffolds. Furthermore, the ability to tailor the chemical composition, uniformity and thickness of the metal oxide shell *via* thermal

decomposition approach of single source precursors was accomplished. The SEM, EDX and XRD analyses confirm that the hierarchical 3D cobalt structures were preserved after removing the template by etching the calcite under mild acidic conditions. Remarkable performances of the *Sorites*@Co and *Sorites*@NiO catalysts, in electrochemical water oxidation reactions, and *Sorites*@Fe(OH)$_x$ filter, in water purification processes, were achieved. The use of the identical and 3D porous structures of fossil scaffolds, corresponding to an abundant and inexpensive source, combined with facile, general, and low-cost coating process using numerous inorganic and organic materials can pave the way for the development of next-generation versatile catalysts, filters, batteries, photonic crystals, etc.

Experimental Section

Materials: Co(ac)$_2$ (99.995%) and Fe(ac)$_2$ (99.995) were purchased from Sigma Aldrich. Mn(ac)$_2$ (98%) and Ni(ac)$_2$·4H$_2$O (>98%) were purchased from Strem. FeSO$_4$·7H$_2$O (99%), hexadecylamine (HDA, 90%), and NaOH (98%) were purchased from Alfa Aesar.

Sorites pre-treatment: *Sorites* were immersed in 0.05 M HCl solution for 2–3 min at room temperature to clean and etch their outermost layer.

Coating with metal oxide nanostructure: Forty mg of M(ac)$_2$ (M: Co, Ni, Fe, Mn) were dissolved in 1 mL HDA. Then, a 20 mL vial which containing the *Sorites* (10 mg) and 500 µL of the metal acetate solution was placed on a heating plate inside a glove box and heated at 270 °C for 20 min, except in the case of cobalt, which was heated at 300 °C for 30 min. The products were cleaned by hexane and dried at 60 °C.

Coating with Fe(OH)$_x$: Ten mL of 0.1 M iron salt (FeSO$_4$·7H$_2$O, pH=3) were added into vial containing 0.5 g *Sorites*. The iron solution was removed after 30 min, and the *Sorites* with the adsorbed iron salt were heated at 90 °C.

Etching process: *Sorites* that were coated with cobalt nanostructures were heated at 550 °C for 5 h to convert Co metal to Co$_3$O$_4$. Then, the cobalt oxide structures were transferred to 0.1 M HCl solution for 30 min for complete etching of the *Sorites* CaCO$_3$.

Working electrode preparation and electrochemical measurements: Electrocatalytic measurement of the *Sorites*@Co and *Sorites*@NiO was carried out in a 1 M aqueous NaOH solution, using a VersaSTAT 3 potentiostat in a three-electrode system. The 3D structures acted as the working electrode, a platinum wire as the counter electrode, and Ag/AgCl in saturated KCl served as the reference electrode, separated by glass frits. The voltage was swept between –0.2 and +1 V *vs*. Ag/AgCl at a scan rate 20 mV/s. Preparation of the working electrode was carried out by pasting the *Sorites*@Co and *Sorites*@NiO to copper electrode using silver paint.

The area of the working electrodes was calculated based on the dimensions of the *Sorites@Co and Sorites@NiO* measured from SEM images as depicted in Figures S2, S3 and Tables 1 and 2).

Atomic absorption spectroscopy (AAS) measurement: The metal concentrations were measured by atomic absorption spectroscopy using Perkin Elmer Analyst 400. The samples were filtered with 0.22 µm syringe filter and measured by the AAS in triplicate. A calibration curve was performed using standard solutions before each measurement.

Instruments: SEM images were recoded using a JEOL SM-7400F ultra-high-resolution electron microscope with a cold-field emission-gun operated at 3.5 kV. EDX was detected using energy-dispersive X-ray (EDX) detector coupled with the SEM, operated at an accelerating voltage of 15 kV. Phase analysis of the samples was carried out using the *X-ray diffraction (XRD) method*. The data were collected on an Empyrean Powder Diffractometer (Panalytical) equipped with a position sensitive (PSD) X'Celerator detector using Cu Kα radiation ($\lambda=1.5418$ Å) and operated at 40 kV and 30 mA. UV−Vis absorbance measurements were taken using a Cary 5000 UV−Vis−NIR spectrophotometer.

References

[1]   J. Gao, Y. Liu, H. Xu, Z. Wang, X. Zhang, *Langmuir* **2009**, *25*, 4365.

[2]   E. K. Payne, N. L. Rosi, C. Xue, C. A. Mirkin, *Angew. Chem, Int. Ed.* **2005**, *44*, 5064.

[3]   S. Kinoshita, S. Yoshioka, K. Kawagoe, *Proc. Biol. Sci.* **2002**, *269*, 1417.

[4]   P. F. Joanna Aizenberg, James C. Weaver, Monica S. Thanawala, Vikram C. Sundar, Daniel E. Morse, *Science* **2005**, *309*, 275.

[5]   C. E. Hamm, R. Merkel, O. Springer, P. Jurkojc, C. Maier, K. Prechtel, V. Smetacek, *Nature* **2003**, *421*, 841.

[6]   X. Gao, L. Jiang, *Nature* **2004**, *432*, 36.

[7]   Y. Li, J. Zhang, S. Zhu, H. Dong, Z. Wang, Z. Sun, J. Guo, B. Yang, *J. Mater. Chem.* **2009**, *19*, 1806.

[8]   J. Huang, X. Wang, Z. L. Wang, *Nano Lett.* **2006**, *6*, 2325.

[9]   H. Zhou, T. Fan, X. Li, J. Ding, D. Zhang, X. Li, Y. Gao, *Eur. J. Inorg. Chem.* **2009**, *2009*, 211.

[10] S. Shian, Y. Cai, M. R. Weatherspoon, S. M. Allan, K. H. Sandhage, *J. Am. Ceram. Soc.* **2006**, *89*, 694.

[11] E. Dujardin, C. Peet, G. Stubbs, J. N. Culver, S. Mann, *Nano Lett.* **2003**, *3*, 413.

[12] W. Shenton, S. Mann, T. Douglas, M. Young, G. Stubbs, *Adv. Mater.* **1999**, *11*, 253.

[13] M. Knez, A. M. Bittner, F. Boes, C. Wege, H. Jeske, E. Maiβ, K. Kern, *Nano Lett.* **2003**, *3*, 1079.

[14] V. Berry, S. Rangaswamy, R. F. Saraf, *Nano Lett.* **2004**, *4*, 939.

[15] D. A. Nanoparticles, Z. Li, S. Chung, J. Nam, D. S. Ginger, C. A. Mirkin, *Angew. Chem. Int. Ed.* **2003**, *115*, 2408.

[16] N. L. Rosi, C. S. Thaxton, C. A. Mirkin, *Angew. Chem. Int. Ed.* **2004**, *43*, 5500.

[17] R. R. Unocic, F. M. Zalar, P. M. Sarosi, Y. Cai, K. H. Sandhage, *Chem. Commun.* **2004**, *1*, 796.

[18] F. Xu, Y. Wang, X. Wang, Y. Zhang, Y. Tang, P. Yang, *Adv. Mater.* **2003**, *15*, 1751.

[19] Y. Wang, Y. Tang, A. Dong, X. Wang, N. Ren, Z. Gao, *J. Mater. Chem.* **2002**, *12*, 1812.

[20] Y. J. Wang, Y. Tang, X. D. Wang, a. G. Dong, W. Shan, Z. Gao, *Chem. Lett.* **2001**, 1118.

[21] M. W. Anderson, S. M. Holmes, N. Hanif, C. S. Cundy, *Angew. Chem. Int. Ed.* **2000**, *39*, 2707.

[22] E. A. Lewis, D. J. Lewis, A. A. Tedstone, G. Kime, S. Hammersley, P. Dawson, D. J. Binks, P. O'Brien, S. J. Haigh, *Chem. Mater.* **2016**, *28*, 5582.

[23] Y. Lang, F. del Monte, B. J. Rodriguez, P. Dockery, D. P. Finn, A. Pandit, *Sci. Rep.* **2013**, *3*, 3205.

[24] B. K. Sen Gupta, *Mod. Foraminifera* **2003**, *36*, 384.

[25] A. R. Loeblich, H. Tappan, *Foraminiferal Genera and Their Classification*, Springer US, Boston, MA, **1988**.

[26] J. W. Murray, *Ecology and Applications of Benthic Foraminifera*, Cambridge University Press, **2006**.

[27] O. F. Z. Khan, P. O'Brien, *Polyhedron* **1991**, *10*, 325.

[28] M. S. Aw, S. Simovic, Y. Yu, J. Addai-mensah, D. Losic, *Powder Technol.* **2012**, *223*, 52.

[29] Z. Bao, M. R. Weatherspoon, S. Shian, Y. Cai, P. D. Graham, S. M. Allan, G. Ahmad, M. B. Dickerson, B. C. Church, Z. Kang, H. W. Abernathy III, C. J. Summers, M. Liu, K. H. Sandhage, *Nature* **2007**, *446*, 172.

[30] J. Q. Dalagan, E. P. Enriquez, L.-J. Li, C.-T. Lin, *Mater. Sci.* **2013**, *31*, 226.

[31] X. L. Guo, M. Kuang, F. Li, X. Y. Liu, Y. X. Zhang, F. Dong, D. Losic, *Electrochim.*

Acta **2016**, *190*, 159.

[32] A. Jantschke, C. Fischer, R. Hensel, H.-G. Braun, E. Brunner, *Nanoscale* **2014**, *6*, 11637.

[33] D. Losic, Y. Yu, M. S. Aw, S. Simovic, B. Thierry, J. Addai-Mensah, *Chem. Commun.* **2010**, *46*, 6323.

[34] Y. Yu, J. Addai-Mensah, D. Losic, *Sci. Technol. Adv. Mater.* **2012**, *13*, 15008.

[35] B. S. Yeo, A. T. Bell, *J. Am. Chem. Soc.* **2011**, *133*, 5587.

[36] Y. Zhao, S. Chen, B. Sun, D. Su, X. Huang, H. Liu, Y. Yan, K. Sun, G. Wang, *Sci. Rep.* **2015**, *5*, 7629.

[37] S. Mao, Z. Wen, T. Huang, Y. Hou, J. Chen, *Energy Environ. Sci.* **2014**, *7*, 609.

[38] P. W. Menezes, A. Indra, D. González-Flores, N. R. Sahraie, I. Zaharieva, M. Schwarze, P. Strasser, H. Dau, M. Driess, *ACS Catal.* **2015**, *5*, 2017.

[39] H. Tüysüz, Y. J. Hwang, S. B. Khan, A. M. Asiri, P. Yang, *Nano Res.* **2013**, *6*, 47.

[40] M. Gong, W. Zhou, M.-C. Tsai, J. Zhou, M. Guan, M.-C. Lin, B. Zhang, Y. Hu, D.-Y. Wang, J. Yang, S. J. Pennycook, B.-J. Hwang, H. Dai, *Nat. Commun.* **2014**, *5*, 4695.

[41] A. Singh, S. L. Y. Chang, R. K. Hocking, U. Bach, L. Spiccia, *Energy Environ. Sci.* **2013**, *6*, 579.

[42] K. Sun, F. H. Saadi, M. F. Lichterman, W. G. Hale, H.-P. Wang, X. Zhou, N. T. Plymale, S. T. Omelchenko, J.-H. He, K. M. Papadantonakis, B. S. Brunschwig, N. S. Lewis, *Proc. Natl. Acad. Sci.* **2015**, *112*, 201423034.

[43] R. Ahmad, R. Kumar, S. Haseeb, *Arab. J. Chem.* **2012**, *5*, 353.

[44] M. Pettinato, S. Chakraborty, H. A. Arafat, V. Calabro, *Ecotoxicol. Environ. Saf.* **2015**, *121*, 57.

[45] Y. Fan, F. Su, K. Li, C. Ke, Y. Yan, *Sci. Rep.* **2017**, *7*, 45643.

[46] C. Park, J. Jung, C. W. Lee, J. Cho, *Sci. Rep.* **2016**, *6*, 39136.

[47] P. N. Dave, L. V Chopda, *J. Nanotechnol.* **2014**, *2014*, 398569/1.

[48] M. Hua, S. Zhang, B. Pan, W. Zhang, L. Lv, Q. Zhang, *J. Hazard. Mater.* **2012**, *211–212*, 317.

[49] T. B. Scott, G. C. Allen, P. J. Heard, A. C. Lewis, D. F. Lee, *Proc. R. Soc. A Math. Phys. Eng. Sci.* **2005**, *461*, 1247.
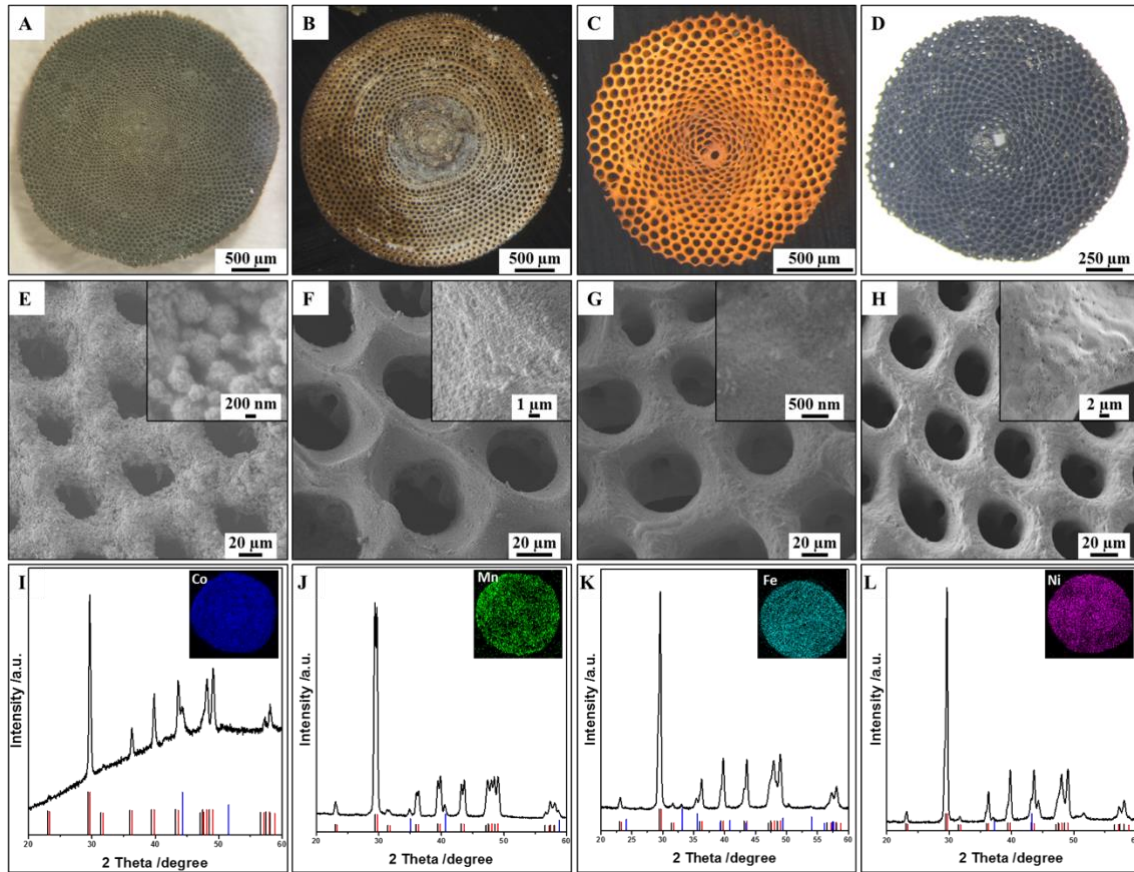
Figure 1. The generality of coating *Sorites* structures with different materials. A–D) Optical images and E–H) SEM images of the *Sorites* coated with Co, MnO, α-Fe$_2$O$_3$, and NiO, respectively. High magnification SEM image of each structure is shown in the inset. I–L) XRD patterns and EDX mapping (inset) of the *Sorites* coated with Co, MnO, α-Fe$_2$O$_3$, and NiO, respectively. The red, black, and blue lines in the XRD spectra correspond to the bulk structures of rhombohedral Mg$_{0.1}$Ca$_{0.9}$CO$_3$, rhombohedral CaCO$_3$, and to the coated materials, respectively.
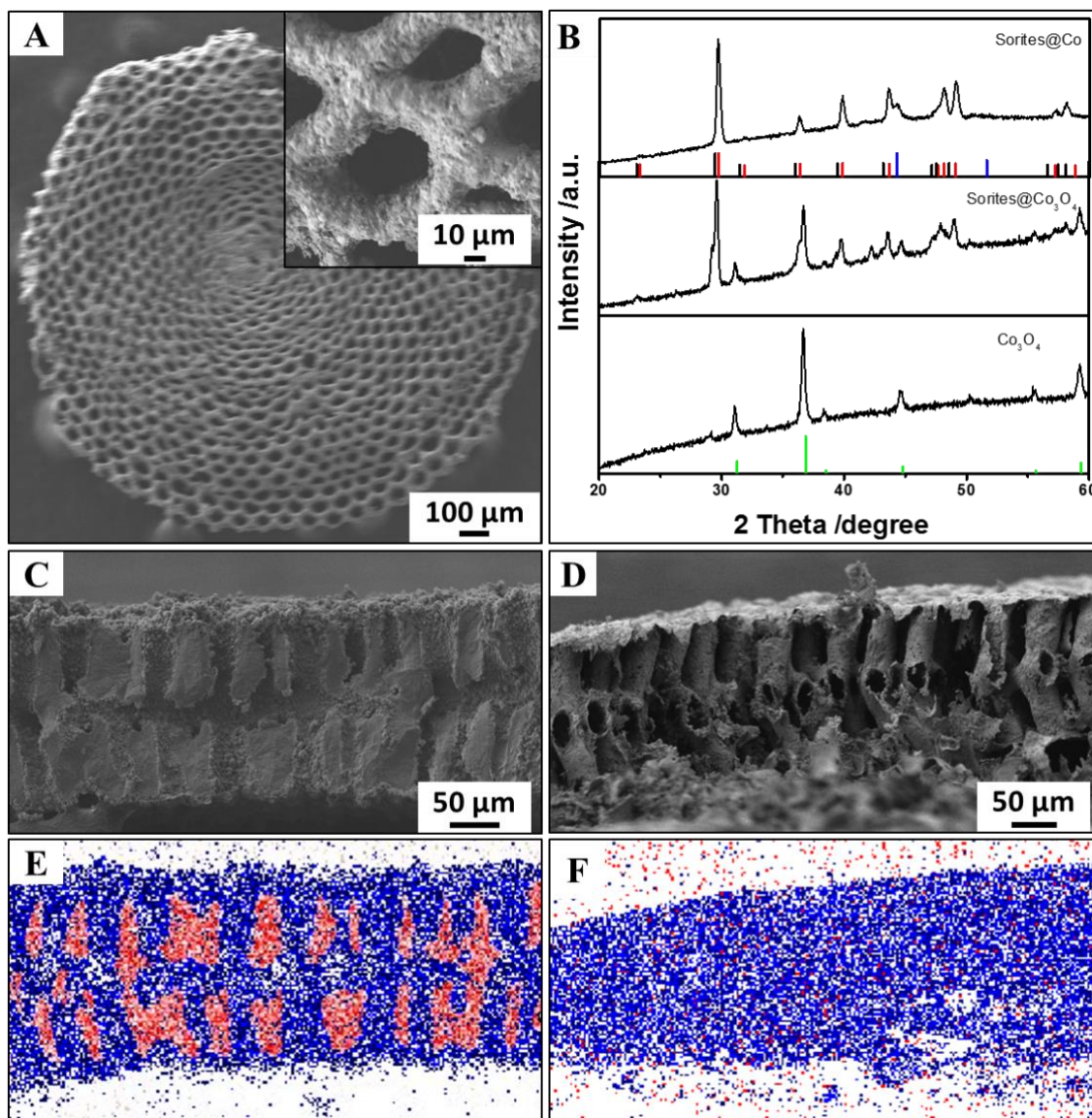
Figure 2. SEM images of the 3D structures before and after removing the $CaCO_3$ template. A) SEM images of top view after etching the *Sorites* templates, B) XRD pattern of *Sorites*@Co (upper pattern), *Sorites*@Co_3O_4 (middle pattern) and pure Co_3O_4 (bottom pattern). The red, black, blue, and green lines in the XRD spectra correspond to the bulk structures of rhombohedral $Mg_{0.1}Ca_{0.9}CO_3$, rhombohedral $CaCO_3$, cubic Co, and Co_3O_4, respectively. (C and D) SEM images of cross section view of the structures, (C) before etching and (D) after etching. EDX mapping of the images shown in (C and D) were taken, (D) before etching and (F) after etching the *Sorites* template. The Ca and Co are colored in red and blue, respectively.
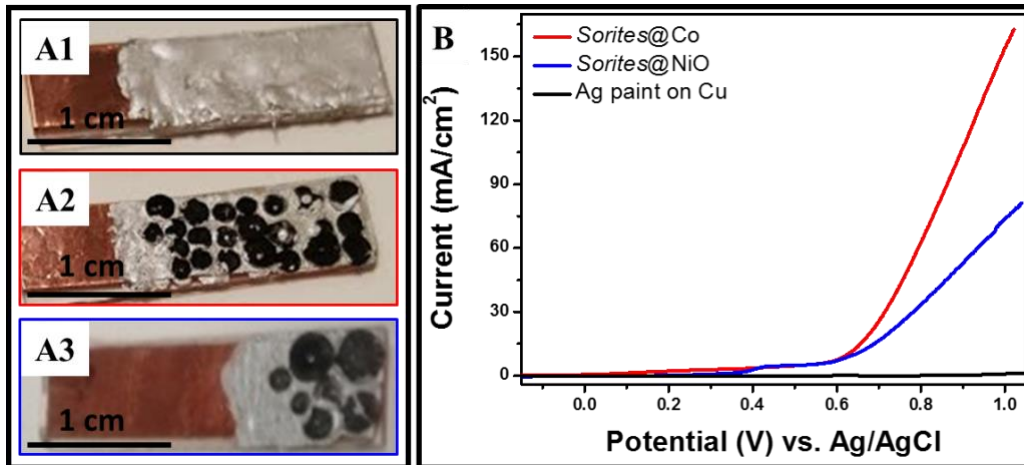
Figure 3. A) Photograph images of the prepared electrodes, on the top (A1) the silver paint, on the middle (A2) *Sorites*@Co, and on the bottom (A3) *Sorites*@NiO. A) *J-V* curve for water oxidation reaction using the *Sorites*@Co (red trace), *Sorites*@NiO (blue trace), and silver paint (black trace) on Cu electrode, with a scan rate of 20 mV/s.
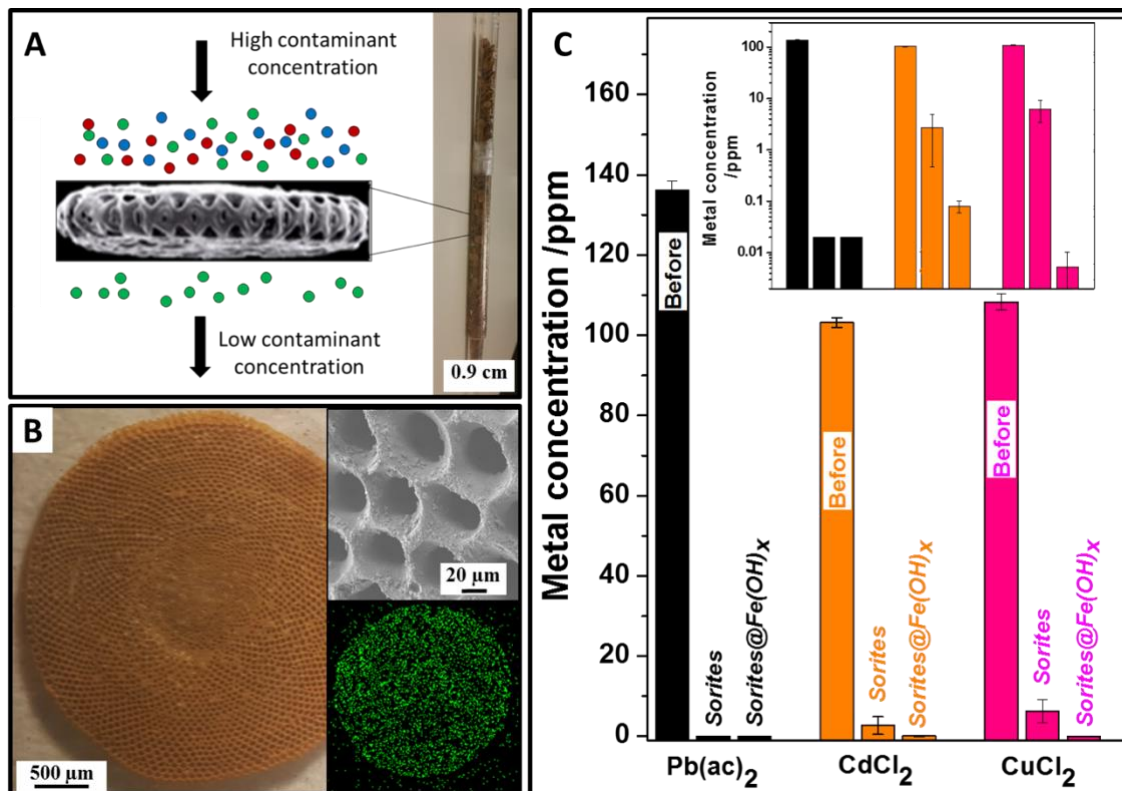
Figure 4. A) Optical image of the filter and a schematic description of the filtration process. B) Optical image of the *Sorites*@Fe(OH)$_x$ and high magnification SEM image and EDX mapping are shown in the insets. C) Three different metal concentration (Pb^{2+} black bars, Cd^{2+} orange bars, and Cu^{2+} pink bars) were filtered through plain *Sorites* and *Sorites*@Fe(OH)$_x$, where the solution concentration were checked before and after the filtration by AA. The insets in C show the concentration of the metal cations before and after filtration in a logarithmic scale. All error bars represent standard deviation from triplicate experiments.